

Functional Latent Dynamics for Irregularly Sampled Time Series Forecasting

Christian Klötergens¹, Vijaya Krishna Yalavarthi¹, Maximilian Stubbemann¹,
and Lars Schmidt-Thieme¹

ISMLL, University of Hildesheim, Germany {kloetergens, yalavarthi,
stubbemann, schmidt-thieme}@ismll.uni-hildesheim.de

Abstract. Irregularly sampled time series with missing values are often observed in multiple real-world applications such as healthcare, climate and astronomy. They pose a significant challenge to standard deep learning models that operate only on fully observed and regularly sampled time series. In order to capture the continuous dynamics of the irregular time series, many models rely on solving an Ordinary Differential Equation (ODE) in the hidden state. These ODE-based models tend to perform slow and require large memory due to sequential operations and a complex ODE solver. As an alternative to complex ODE-based models, we propose a family of models called Functional Latent Dynamics (FLD). Instead of solving the ODE, we use simple curves which exist at all time points to specify the continuous latent state in the model. The coefficients of these curves are learned only from the observed values in the time series ignoring the missing values. Through extensive experiments, we demonstrate that FLD achieves better performance compared to the best ODE-based model while reducing the runtime and memory overhead. Specifically, FLD requires an order of magnitude less time to infer the forecasts compared to the best performing forecasting model.

Keywords: Irregularly Sampled Time Series · Missing Values · Forecasting

1 Introduction

Time series forecasting plays a pivotal role in numerous fields, ranging from finance and economics to environmental science and healthcare. A time series is considered multivariate if multiple variables, also known as channels, are observed. In the realm of time series forecasting, most of the literature considers *regular time series*, where the time difference between the observed points is equal, and no observations are missing. However, in real-world application such as in healthcare domains, different channels are often independently and irregularly observed leading to an extremely sparse multivariate time series when they are aligned. We refer to these time series as Irregularly Sampled Multivariate Time Series with missing values (IMTS). The forecasting task of regular multivariate time series and IMTS is illustrated in Figure 1.

Forecasting of IMTS is not well-covered in the literature compared to forecasting of regular time series. Machine learning models that are designed for forecasting regular multivariate time series often rely on the relative position of the observation in the series rather than the absolute time, and cannot accommodate missing values. Applying these models to IMTS forecasting is not trivial. More specific, models need to implement strategies to handle varying observation distances and missing values. The standard method of handling missing values is imputation. However, this approach is usually suboptimal as absence of data itself carries information, which is discarded by imputation. Additionally, imputation errors accumulate and heavily affect the final forecasting task. Therefore, IMTS models must incorporate a more advanced method to handle missing values and directly take observation times into account.

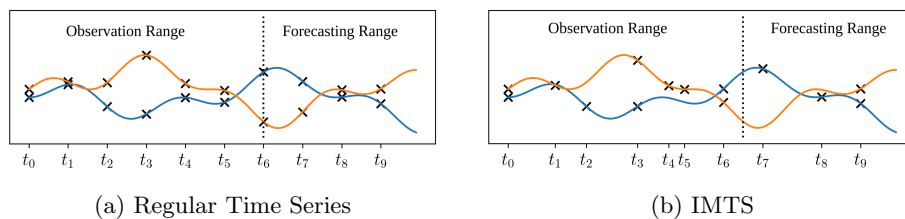


Fig. 1: Example for regularly and irregularly sampled Time Series with three channels. The observations and forecasting targets are marked as black crosses.

Ordinary Differential Equation (ODE)-based models [2,3,1,12,11] have been widely studied for this task. These models capture underlying dynamics of continuous time, making them well-suited for IMTS forecasting where the time intervals between observations vary. However, ODE-based models cannot directly handle the missing values, a prevalent occurrence in various application scenarios. Furthermore, they are inefficient in terms of run time as they operate in sequential manner similar to recurrent neural networks (RNNs).

In this work, we propose a novel family of models called **F**unctional **L**atent **D**ynamics (FLD). The hidden states of FLD are governed by a function whose coefficients are derived from the observed time series. The hidden state function can be any curve such as a polynomial or sine function. As the hidden state function accepts continuous time points as inputs, it can be evaluated at any desired time. Our encoder considers only observed values in the time series and ignores the missing values to parameterize the hidden state function. Finally, a dense fully connected deep neural network is applied to the hidden state to obtain the forecasts.

Our approach is capable of utilizing any type of parameterized, differentiable function and can thus be adapted to various forecasting scenarios.

FLD serves as an alternative to ODE-based models and can handle both missing values and irregular sampling. By employing simple curve functions to

model hidden state dynamics, we demonstrate that the forecasting accuracy of FLD is significantly better than ODE based models and competitive with the state-of-the-art IMTS forecasting models on 4 real-world IMTS datasets. Additional studies on computational efficiency show that FLD significantly outperforms competing models in terms of inference time. Our contributions are as follows.

- We propose Functional Latent Dynamics (FLD), a novel method for IMTS forecasting. FLD captures latent dynamics in a continuous fashion with parameterized curve functions.
- We propose an approach to incorporate the well-established attention mechanism to learn the coefficients of our curve functions that encode the IMTS.
- We provide a Proof-of-Concept on a simple toy datasets task that is generated with the Goodwin oscillator model [4], an ODE designed to model enzyme synthesis.
- We conduct extensive experiments on established benchmark tasks. Our results indicate that FLD outperforms state-of-the-art competitors by an order of magnitude in terms of inference time while providing competitive forecasting accuracy.

Our code is publicly available on an anonymous Git repository: <https://anonymous.4open.science/r/Functional-Latent-Dynamics-5B1E/>

2 Problem Formulation

An *Irregularly sampled multivariate time series (IMTS)* is a sequence $x := ((t_1, v_1), \dots, (t_N, v_N))$ of N many pairs where each pair consists of an observation time point $t_n \in \mathbb{R}$ and observation event $v_n \in X^C := (\mathbb{R} \cup \{\text{NaN}\})^C$ made at t_n ; $C \in \mathbb{N}$ is the number of channels, $v_{n,c} \neq \text{NaN}$ represents a *observed value* and $v_{n,c} = \text{NaN}$ represents a *missing value*. An *IMTS forecasting query* is a sequence $t^q := (t_1^q, \dots, t_K^q)$ of time points for which observation values are sought (where $\min_{k=1:K} t_k^q > \max_{n=1:N} t_n$). Any sequence $y := (y_1, \dots, y_K)$ of same length with values in X^C we call an *IMTS forecasting answer*. To measure the difference between the ground truth forecasting answer y (possibly with missing values) and the predicted forecasting answer \hat{y} (without missing values), a scalar loss function $\ell : \mathbb{R} \times \mathbb{R} \rightarrow \mathbb{R}$ such as squared error is averaged over all query time points and non-missing observations:

$$\ell(y, \hat{y}) := \frac{1}{\sum_{k=1}^K N_k} \sum_{k=1}^K \sum_{\substack{c=1 \\ y_{k,c} \neq \text{NaN}}}^C \ell(y_{k,c}, \hat{y}_{k,c}),$$

where $N_k = |\{c \in [C] \mid y_{k,c} \neq \text{NaN}\}|$ denotes the amount of non-missing values of the forecasting answer y_k at time point t_k^q .

An *IMTS forecasting dataset* consists of M many triples (x_m, t_m^q, y_m) (called instances) consisting of a past IMTS x_m , a query t_m^q of future time points and

the ground truth observation values y_m for those time points, drawn from an unknown distribution ρ . The length N of the past and the number K of queries will vary across instances in general, while the number C of channels is the same for all instances.

The *IMTS forecasting problem* then is, given such a dataset $D := ((x_1, t_1^q, y_1), \dots, (x_M, t_M^q, y_M))$ and a loss function ℓ , find a model $\mathcal{M} : (X^C)^* \times \mathbb{R}^* \rightarrow (\mathbb{R}^C)^*$, where $*$ denotes finite sequences, such that its expected forecasting loss is minimal:

$$\mathcal{L}(\mathcal{M}; \rho) := \mathbb{E}_{(x, t^q, y) \sim \rho} [\ell(y, \mathcal{M}(x, t^q))]$$

3 Background

ODE-based models [2,3,1,11,12] are a family of continuous-time models wherein the hidden state $z(\tau)$ is the solution of an initial value problem in Ordinary Differential Equations (ODEs):

$$\frac{dz(\tau)}{d\tau} = f(\tau, z(\tau)) \quad \text{where} \quad z(\tau_0) = z_0 \quad (1)$$

Here, τ can both reference to observation time points t and query time points t^q . f is a trainable neural network that governs the dynamics of the hidden state. The hidden state $z(\tau)$ is defined at all times and can be evaluated at any desired time-points. Hence, they are a natural fit to model IMTS, where observation times are continuous. However, a numerical ODE solver is required to infer the hidden state:

$$z_0, \dots, z_N := \text{ODESolve}(f, z_0, (\tau_0, \dots, \tau_N)) \quad (2)$$

Here, z_n is the hidden state for τ_n and z_0 is the initial value.

GRU-ODE-Bayes [3] integrates a continuous version of Gated Recurrent Units (GRU) into the neural ODE architecture and updates $z(t)$ with Bayesian inference based.

LinODENet [12] replaces the neural ODE with a linear ODE, in which the ODE solutions are computed by a linear layer. Using a linear ODE enables the model to omit the ODE solver. For updates at observations, LinODENet model incorporates Kalman filtering to ensure the self-consistency property, where the state of the model only changes when the observation deviates from the model prediction.

Continuous Recurrent Units (CRU) [11] replace the ODE with a Stochastic Differential Equation (SDE). Using an SDE has the benefit that the change of latent state over any time frame can be computed in closed form with continuous-discrete Kalman filtering.

Related to neural ODE, Neural Flows [1] apply invertible networks to directly model the solution curves of ODEs, rendering the ODE solver obsolete.

While ODE-based models have the advantage of learning from continuous time observations, they require complex numerical ODE solver which is slow [1].

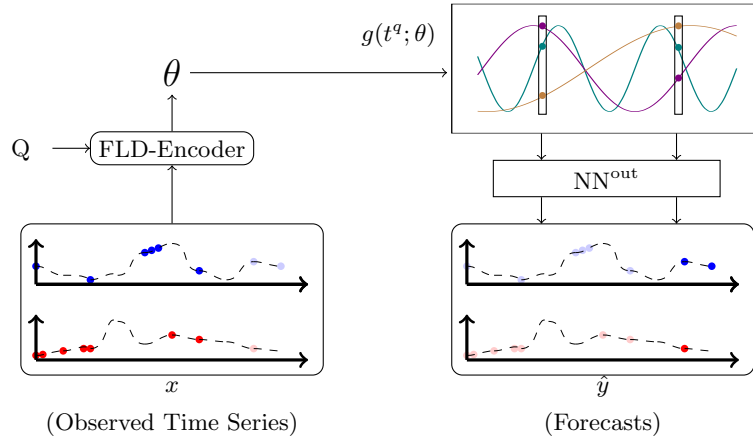


Fig. 2: Example of FLD with sine functions as a 3-dimensional hidden state. The parameters θ of the hidden state function $g(\cdot; \theta)$ are inferred by aggregating the observations (red/blue dots) with the attention-based FLD-Encoder. The hidden state at the query times is acquired by following $g(t^q; \theta)$ and decoded by a neural network (NN^{out}).

Additionally, they process the observations of an IMTS sequentially worsening the run time and also increase the memory requirements. Furthermore, ODE-based models cannot directly handle missing values. Typically, they require missing value indicators which act as additional input channels in the series complicating the learning process.

Substantially different from neural ODEs, GraFITi [17] encodes time series as graphs and solves the forecasting problem using graph neural networks. The model showed superior forecasting accuracy on the established benchmark datasets, while having significantly faster inference than ODE-based models.

4 Functional Latent Dynamics

We introduce a family of models called Functional Latent Dynamics as an alternative to ODE-based models. Here, we use simple curves to specify the hidden state. Specifically, we replace ODESolve in eq. (2) with curves such as polynomial or sine functions. The latent state z_n is given as:

$$z_n := g(\tau_n; \theta)$$

where g is a curve with coefficients θ .

Inferring the hidden state at any time point with a function is computationally efficient if that function is simple and does not depend on other time points. Large portion of the literature applies sequential models such as RNNs to learn the inductive bias from the causal nature of time series. However, they

Algorithm 1 Functional Linear Dynamics

Require: Observed IMTS x , Query time points t^q , latent function g

- 1: $\theta \leftarrow \text{FLD-Encoder}(x)$ {▷ Compute the function coefficients}
- 2: **for** $k = 1, \dots, K$ **do**
- 3: $z_k \leftarrow g(t_k^q, \theta)$ {▷ Compute the latent state}
- 4: $\hat{y}_k \leftarrow \text{NN}^{\text{out}}(z_k)$ {▷ Make the prediction}
- 5: **return** $(\hat{y}_k)_{k=1:K}$

are slow, as they have to operate sequentially. Alternatively, recent transformer based works in similar domains [10,15] show that we can achieve state-of-the-art performance even without applying the sequential model. Hence, in this work, we use simple curves such as polynomial (linear in eq. (3), quadratic in eq. (4)) or sine functions (in eq. (5)).

$$g^{\text{lin}}(t; \theta) := \theta_1 t + \theta_2 \quad \theta = (\theta_1, \theta_2) \in \mathbb{R}^{2 \times L} \quad (3)$$

$$g^{\text{quad}}(t; \theta) := \theta_1 t^2 + \theta_2 t + \theta_3 \quad \theta = (\theta_1, \theta_2, \theta_3) \in \mathbb{R}^{3 \times L} \quad (4)$$

$$g^{\text{sin}}(t; \theta) := \theta_1 \sin(\theta_2 + \theta_3 t) + \theta_4 \quad \theta = (\theta_1, \theta_2, \theta_3, \theta_4) \in \mathbb{R}^{4 \times L} \quad (5)$$

Here, *sin* is applied coordinate-wise. Once we compute the latent state z , we apply a multilayer feedforward neural network (NN^{out}) to compute \hat{y} via

$$\hat{y}_k = \text{NN}^{\text{out}}(z_k).$$

5 Inferring Coefficients

Values of θ are computed from the observed time series X using the FLD-Encoder. First, we convert x into C many tuples $x^{(1)}, \dots, x^{(C)}$ where $x^{(c)} = (t^{(c)}, v^{(c)})$. Here, $t^{(c)} = (t_1^{(c)}, \dots, t_{N_c}^{(c)})$ and $v^{(c)} = (v_1^{(c)}, \dots, v_{N_c}^{(c)})$ represent the observation time points and values in channel c , respectively, i.e., the time points with no missing values in channel c and the corresponding values. We pass all the tuples $x^{(c)}$ to a multi-head attention based encoder. We begin with time embeddings.

Continuous time embeddings. Our attention-based FLD-Encoder consists of H many heads and for each head h , we provide a D dimensional embedding $\phi^h : \mathbb{R} \rightarrow \mathbb{R}^D$ of time points:

$$\phi_d^h(t) := \begin{cases} a_{di}t + b_{di} & \text{if } d = 1 \\ \sin(a_{di}t + b_{di}) & \text{if } 1 < d \leq D \end{cases} \quad (6)$$

Here, a_{di} and b_{di} are trainable parameters. This embedding helps to learn periodic terms from the sinusoidal embeddings and non-periodic terms from the linear embedding [13].

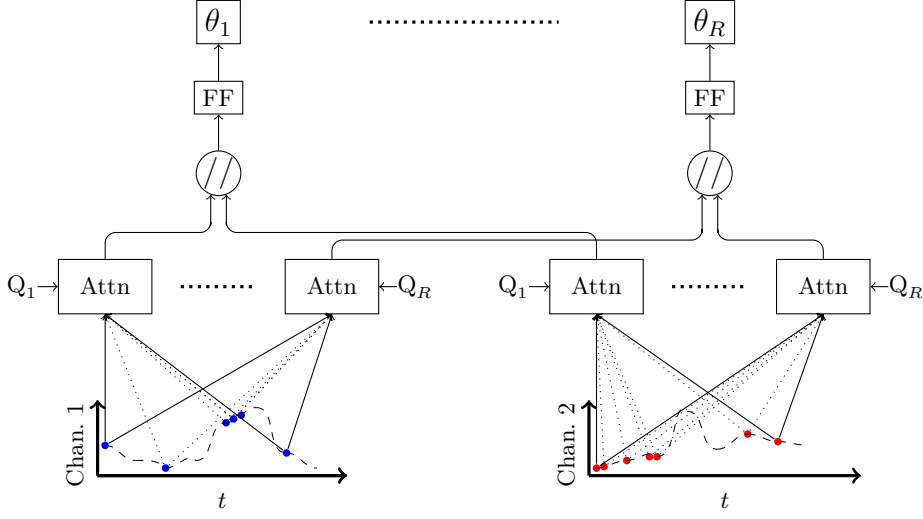


Fig. 3: FLD-Encoder infers coefficients θ to model the hidden dynamics of an IMTS. The channel observations are aggregated with attention (Attn), concatenated (//) and combined with a feed forward layer (FF).

Multi-head attention encoder. In the following, $Q^h \in \mathbb{R}^{R \times D}$ is a matrix of trainable parameters where Q_r^h provides vector representation to θ_r , $R = |\theta|$. $K^{h,c} := \phi_h(t^{(c)})$ is the continuous embedding of time points in $t^{(c)}$, and $V^c = v^{(c)}$. $\text{FF} : \mathbb{R}^{HC} \rightarrow \mathbb{R}^L$ is a single feed forward layer. Note that similar to scaled dot-product attention in [16], softmax is applied row wise.

Presence of missing values in the data makes it challenging to apply multi-head attention directly. Hence, we modify it as follows:

$$\begin{aligned}
 \theta &:= \text{FF}(\hat{\theta}) && \in \mathbb{R}^{R \times L} \\
 \hat{\theta} &:= [\hat{\theta}^{1,1}, \dots, \hat{\theta}^{1,C}, \dots, \hat{\theta}^{H,1}, \dots, \hat{\theta}^{H,C}] && \in \mathbb{R}^{R \times HC} \\
 \hat{\theta}^{h,c} &:= A^{h,c} V^c && \in \mathbb{R}^{R \times 1} \\
 A^{h,c} &:= \text{softmax} \left(Q^h \left(K^{h,c} \right)^T / \sqrt{D} \right) && \in \mathbb{R}^{R \times |N_c|}
 \end{aligned}$$

A forward pass of IMTS forecasting using the proposed model is presented in Algorithm 1.

Delineating from mTAN Encoder. Our encoder shares some features with the mTAN encoder [13]. The mTAN encoder is used to convert an IMTS into a fully observed regularly sampled time series in the latent space. Instead, the goal of our encoder is to compute the coefficients θ instead of converting to another time series. Hence, our attention query is a trainable matrix instead of embedded reference time points.

6 Modelling Goodwin Oscillators with FLD-L

FLD operates on the assumption that complex functions can be modeled by combining multiple simple curves with a deep neural network. To investigate FLD-L’s ability to learn non-linear dynamics, we conduct an experiment with time series generated by the Goodwin oscillator model [4], which describes negative feedback interactions of cells at the molecular level.

For our experiments we use the implementation that was published in CellML [8]. The dataset samples have two input channels and were generated by varying the constants and initial states of the Goodwin oscillator. Figure 4a shows a sample generated by the oscillator and FLD-L’s prediction. Furthermore, we plot the hidden states that the trained FLD-L model inferred for that sample in Figure 4b. The experiment on the synthetic Goodwin dataset demonstrates that FLD is capable to precisely infer a non-linear time series, although the hidden states develop linearly over time.

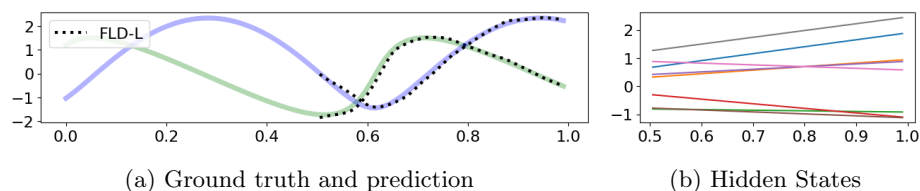


Fig. 4: Experiment on synthetic data created by the Goodwin oscillator model. We show FLD-L’s forecast (left) and the inferred hidden states (right).

7 Benchmark Experiments

We provide details about the tasks, datasets, and models that were used in our experiments. To ensure a fair comparison with previous work, we utilize established benchmark datasets and protocols.

7.1 Datasets

Following the IMTS forecasting literature [3,1,17,12], we conduct experiments on four different datasets USHCN, Physionet-2012, MIMIC-III and MIMIC-IV.

USHCN [9] contains measurements of 5 variables from 1280 weather stations in the USA. Following the preprocessing proposed by DeBrouwer et al. [3], most of the 150+ years of observation time is ignored and only measurements from 1996-2000 are used in the experiments. Furthermore, USHCN is made sparse artificially by only keeping a randomly sampled 5% of the measurements.

Physionet-2012 [14] comprises a dataset consisting of the medical records of 12,000 ICU-patients. During the initial 48 hours of admission, measurements

Table 1: Statistics of data sets used for experiments. *Max. Len.* refers to the maximum sequence length among samples. *Max. Obs.* refers to the maximum number of non-missing observations among samples. *Sparsity* refers to the percentage of missing values over all samples.

Name	#Sampl.	#Chann.	Max. Len	Max. Obs	Spars.
USHCN	1.114	5	370	398	78.0%
Physionet-2012	11.981	37	48	606	80.4%
MIMIC-III	21.250	96	97	677	94.2%
MIMIC-IV	17.874	102	920	1642	97.8%

of 37 vital signs were recorded. Following the approach used in previous studies [3,1,17,12], we pre-process the dataset to create hourly observations, resulting in a maximum of 48 observations in each series.

MIMIC-III [5] is a widely utilized medical dataset that provides valuable insights into the care of ICU patients. In order to capture a diverse range of patient characteristics and medical conditions, 96 variables were meticulously observed and documented. To ensure consistency, we followed the preprocessing steps outlined in previous studies [1, 3, 11]. Specifically, we round the recorded observations into 30-minute intervals and only use observations from the 48 hours following the admission. Patients who spend less than 48 hours in the ICU are disregarded.

MIMIC-IV [6] represents an expansion and improvement over MIMIC-III, offering an updated and enriched dataset that enables more comprehensive exploration and analysis. It incorporates new data sources and additional patient records, providing an enhanced foundation for researchers to delve into temporal patterns, forecast future medical events, and gain valuable insights into critical care management. Strictly following [1,17], we preprocess MIMIC-IV similar to MIMIC-III, but round observations into 1-minute intervals.

7.2 Competing models

We compare FLD models against members of the neural ODE family: **GRU-ODE-Bayes** [3], **Neural Flows** [1], **LinODENet** [12], **CRU** [11]. Besides the ODE-based models, we also compare our results to **GraFITi** [17], the state-of-the-art in IMTS forecasting model.

mTAN [13] was not introduced as a forecasting model, but we still selected the model as one of our competitors, because the FLD-Encoder is related to the mTAN encoder. The model is trained using the training routine that was originally proposed for interpolation purposes. In the experimental results of this work, mTAN refers to the mTAND-Full architecture, as described by Shukla et al. [13].

Table 2: FLD’s hyperparameter search space for the benchmark experiments

Hyperparameter	Search Space
Hidden Dimension	{32,128,256,512}
Attention Heads	{4,8}
Decoder Depth	{2,4}
Embedding Size per Attention Head	{2,4,8}

7.3 Task Protocol

We adopted the experimental protocol as published by Yalavarthi et al. [17]. Our experiments on IMTS forecasting involve varying the observation range and forecasting horizon across multiple tasks for each dataset to assess different model capabilities. The widely used 75%-3 task requires models to predict the next three time steps after observing 75% of the time series, equating to 36 hours for healthcare datasets and the first three years for the USHCN dataset. To challenge models with a longer forecasting horizon, we also undertake the 50%-50% task, where models predict the second half of an IMTS using the first half as observations, meaning 24 hours of prediction for medical datasets and 2 years for the USHCN dataset. Additionally, we also evaluate the models on the 75%-25% to add a task in between the two previous tasks. Here, models see the observations from the initial 36h / 3 years and forecast the remaining 12h / 1 year. For hyperparameter search and early stopping we take a validation set, consisting of 20% of the available data. Furthermore, we set aside another 10% of the data as unseen for the final evaluation (Test Data). We applied 5-fold cross-validation. Each fold reserves different subsets for validation and testing.

The implementation of the experiments are mainly based on the TSDM package provided by Scholz et al. [12]. We run our experiments on Nvidia 2080TI GPU with 12GB.

7.4 Hyperparameters

Regarding hyperparameter optimization for competing models, we use the same hyperparameter search spaces and optimization protocol as introduced by Yalavarthi et al. [17]. For each task, we randomly sample a maximum of 10 sets of hyperparameters and fully train models with the respective configurations on one fold. We select the model with the lowest MSE on the validation data of that fold and then train it on each of the 5 folds to compute the mean and standard deviation of the test loss. The search space for the FLD models is described in table 2. While we vary the number of hidden layers in the decoder networks, we fix the width of each layer at the dimension of the hidden states z .

For all models we use ADAM optimizer [7]. For our models we use an initial learning rate of 0.0001. Furthermore, we add an L2-regularization of weight 0.001.

Table 3: Test MSE for forecasting next three time steps after 75% observation time. OOM refers to out of memory. †: results reported by Yalavarthi et al. [17]. We highlight the best model in **bold** and the second best in *italics*

	USHCN	Physionet-12	MIMIC-III	MIMIC-IV
GraFITi †	0.272 ± 0.047	0.286 ± 0.001	0.396 ± 0.030	0.225 ± 0.001
mTAN †	0.300 ± 0.038	0.315 ± 0.002	0.540 ± 0.036	OOM
GRU-ODE †	0.401 ± 0.089	0.329 ± 0.004	0.476 ± 0.043	0.360 ± 0.001
Neural Flow †	0.414 ± 0.102	0.326 ± 0.004	0.477 ± 0.041	0.354 ± 0.001
LinODE †	0.300 ± 0.060	0.299 ± 0.001	0.446 ± 0.033	<i>0.272 ± 0.002</i>
CRU †	0.290 ± 0.060	0.379 ± 0.003	0.592 ± 0.049	OOM
FLD-L	<i>0.262 ± 0.040</i>	<i>0.297 ± 0.000</i>	<i>0.444 ± 0.027</i>	0.274 ± 0.000
FLD-Q	0.258 ± 0.043	0.301 ± 0.000	0.451 ± 0.024	0.280 ± 0.000
FLD-S	0.282 ± 0.030	0.307 ± 0.000	0.450 ± 0.029	0.313 ± 0.002

7.5 Results

We compare the forecasting accuracy of FLD-L, FLD-Q and FLD-S with that of the competition by conducting experiments using various observation times and forecasting horizons. Since we follow the experimental protocols from [17], we report their results whenever it is possible and run those experiments that have not been conducted yet.

Table 4: Test MSE for forecasting next 25% after 75% observation time. OOM refers to out of memory. †: results reported by Yalavarthi et al. [17]. We highlight the best model in **bold** and the second best in *italics*

	USHCN	Physionet-12	MIMIC-III	MIMIC-IV
GraFITi	0.499 ± 0.152	<i>0.365 ± 0.001</i> †	0.438 ± 0.014 †	0.285 ± 0.002 †
mTAN	0.579 ± 0.182	0.514 ± 0.017	0.985 ± 0.055	OOM
GRU-ODE †	0.914 ± 0.343	0.432 ± 0.003†	0.591 ± 0.018†	0.366 ± 0.154†
Neural Flow	1.019 ± 0.338	0.431 ± 0.001†	0.588 ± 0.014†	0.465 ± 0.003†
LinODenet	0.923 ± 0.877	0.373 ± 0.001†	0.477 ± 0.021†	0.335 ± 0.002†
CRU	0.549 ± 0.238	0.435 ± 0.001†	0.575 ± 0.020†	OOM
FLD-L	0.645 ± 0.150	0.360 ± 0.001	<i>0.552 ± 0.032</i>	<i>0.321 ± 0.000</i>
FLD-Q	0.601 ± 0.097	0.366 ± 0.000	0.559 ± 0.028	0.336 ± 0.000
FLD-S	<i>0.526 ± 0.205</i>	0.366 ± 0.000	0.558 ± 0.033	0.347 ± 0.001

Table 3, Table 4 and Table 5 show the Test MSEs for each model on the 75%-3, 75%-25% and 50%-50% task respectively. Based on our results we do

not observe an FLD variant which consistently outperforms the other two members of the model family. For most datasets, FLD-L shows to be the best fit for the short and medium forecasting range, while FLD-S has the best accuracy on two datasets for the 50%-50% task among FLD variants. FLD-Q makes the best predictions on USHCN for the 75%-3 task, where it even surpasses the state-of-the art model GraFITi [17]. However, USHCN carries large standard deviations across all models and task, especially for the longer forecasting ranges. Consequently, findings on this dataset are less conclusive. GraFITi reports superior forecasting accuracy’s on 10 out twelve dataset/task combinations, but on Physionet-2012 and the 75%-25% task FLD-L improves on GraFITi making it the state-of-the art in this part of the evaluation. When we compare FLD’s performance to the ODE-based models, we observe that the most accurate FLD variant outperforms the best ODE-based models in 7 out of 12 cases. In particular, LinODENet outperforms, FLD on all datasets for the 50%-50% task.

Table 5: Test MSE for forecasting next 50% after 50% observation time. OOM refers to out of memory. †: results reported by Yalavarthi et al. [17]. We highlight the best model in **bold** and the second best in *italics*

	USHCN	Physionet-12	MIMIC-III	MIMIC-IV
GraFITi	0.623 ± 0.153	0.401 ± 0.001 [†]	0.491 ± 0.014 [†]	0.285 ± 0.002 [†]
mTAN	<i>0.721 ± 0.198</i>	0.632 ± 0.023	1.016 ± 0.084	OOM
GRU-ODE [†]	1.019 ± 0.342	0.505 ± 0.001 [†]	0.653 ± 0.023 [†]	0.439 ± 0.003 [†]
Neural Flow	1.019 ± 0.338	0.506 ± 0.002 [†]	0.651 ± 0.017 [†]	0.465 ± 0.003 [†]
LinODENet	0.724 ± 0.185	<i>0.411 ± 0.001</i> [†]	<i>0.531 ± 0.022</i> [†]	<i>0.336 ± 0.002</i> [†]
CRU	0.729 ± 0.185	0.467 ± 0.002 [†]	0.619 ± 0.028 [†]	OOM
FLD-L	0.874 ± 0.212	0.415 ± 0.000	0.545 ± 0.026	0.346 ± 0.001
FLD-Q	0.888 ± 0.236	0.424 ± 0.000	0.554 ± 0.025	0.358 ± 0.000
FLD-S	1.141 ± 1.163	0.414 ± 0.000	0.536 ± 0.023	0.359 ± 0.001

8 Efficiency

We evaluate FLD’s efficiency with respect to inference time. For that experiment each benchmark model is trained on the 50%-50% task of the Physionet-2012, MIMIC-III, MIMIC-IV, and USHCN datasets.

Efficiency comparison of machine learning models is a complex task, since different hyperparameter configurations may introduce a trade-off between number of parameters and prediction accuracy. Scholars typically compare the inference time of hyperparameter sets that were trained to optimize the training objective, in our case forecasting accuracy. However, we argue that this strategy is

not necessarily fair to all models, since it ignores the trade-off between efficiency and accuracy. For example, there might exist a hyperparameter configuration that is barely suboptimal with regard to accuracy, but excels in terms of inference time. Consequently, we compare our model to the fastest hyperparameter configuration from each architecture’s search space. This will provide a lower bound of inference time for the competing models and is only unfair to FLD.

Table 6: Comparison of inference time in seconds on the 50%-50% task. OOM indicates a memory error.

	USHCN	Physionet-12	MIMIC-III	MIMIC-IV
GraFITi	0.176	2.775	3.640	6.719
mTAN	0.062	0.776	1.068	3.494
GRU-ODE	5.378	38.118	46.272	154.543
Neural Flow	1.630	2.835	6.428	44.187
f-CRU	1.657	4.578	9.281	OOM
LinODE	2.852	6.294	13.776	95.050
FLD-L	0.018	0.237	0.394	2.141
FLD-Q	0.020	0.243	0.431	2.380
FLD-S	0.021	0.245	0.435	2.740

We assume that for each model the smallest hyperparameter instances provide the fastest inference. For example, with Neural Flows [1], we use only 1 flow layer, as employing multiple flow layers leads to slower inference and training. We opt for the *euler* solver instead of the *dopri5* solver due to its significantly faster inference, to infer the hidden state of GRU-ODE-Bayes [3]. Additionally, we use the *fast* variant of CRU (f-CRU), that was introduced by Schirmer et al. [11]. For FLD-L, we use the hyperparameter set that has been tuned on validation loss for each task because we found a negligible change in computational speed for different hyperparameters. Table 6 reports the inference time of each model on various datasets. More specific, we refer to the wall-clock time to predict the complete test data of each dataset, with a batch size of 64. We observe that FLD-L infers predictions significantly faster than the competing models. Since mTAN is the second-fastest model, we conclude that FLD’s speed is related to the performant attention-based encoder, since it is closely related with the mTAN encoder. FLD’s inference with parameterized curves results in fewer operations and a significant gain in computational speed. Furthermore, keep in mind that mTAN’s inference time increases drastically if we add more reference points and parameters.

To gain more insight into the trade-off between inference time and forecasting accuracy, we conduct a more detailed efficiency comparison. In Figure 5 we plot validation MSE and inference time of 10 randomly sampled hyperparameter

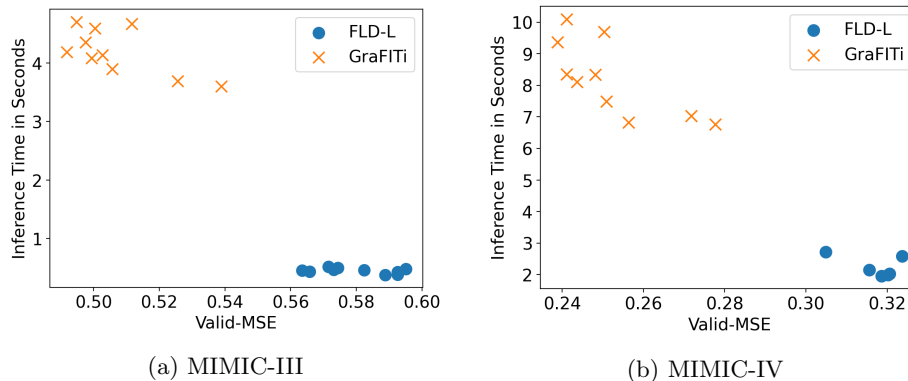


Fig. 5: Efficiency comparison of FLD-L and GraFITi. We plot the validation loss and inference time for 10 randomly sampled hyperparameter configurations for each GraFITi and FLD-L. The plots refer to results on the 75%-25% task on MIMIC-III and MIMIC-IV.

configurations of FLD-L and GraFITi on the two largest datasets MIMIC-III and MIMIC-IV. The plot shows that all versions of FLD-L were significantly faster than GraFITi. However, they were also constantly inferior with respect to forecasting accuracy.

9 Conclusion and Future Work

In this work, we introduced a novel approach to forecast irregularly sampled multivariate time series (IMTS). In particular, we proposed Functional Latent Dynamics (FLD), a model family that models the hidden state of an IMTS with a continuous curve function. This serves as an efficient and accurate alternative to ODE-based models, which have to solve complex differential equations. To be more specific, we outperform all ODE-based models in task with a short and medium forecasting range. Additionally, we surpass the IMTS forecasting state-of-the-art model GraFITi [17] on 2 of 12 evaluation tasks. Our models have magnitudes faster inference speed when compared to ODE approaches, and multitudes faster inference speed than GraFITi.

Our FLD-Encoder can elegantly handle missing observations in order to compute the coefficients of the curve functions. Even if the hidden states are linear, FLD can learn to forecast non-linear functions since non-linearity is induced by its decoder. We demonstrate that hidden states that follow linear curve functions are expressive enough to imitate Goodwin oscillators.

In the future, we will tackle the problem of combining different forms of curve functions like sine and linear curves. Here, the distant vision is to *learn* which kind of curves are appropriate for a specific time-series dataset. As our results indicate that FLD is a performant approach for time-series forecasting, it is

promising to transfer it to probabilistic forecasting settings. Here, it is crucial to derive possibilities for FLD to output distributions instead of point predictions. To achieve this, FLD can, for example, be used as an encoder for a conditioning input for a normalizing flow.

References

1. Biloš, M., Sommer, J., Rangapuram, S.S., Januschowski, T., Günnemann, S.: Neural flows: Efficient alternative to neural odes. *Advances in Neural Information Processing Systems* **34**, 21325–21337 (2021)
2. Chen, R.T.Q., Rubanova, Y., Bettencourt, J., Duvenaud, D.K.: Neural ordinary differential equations. In: Bengio, S., Wallach, H., Larochelle, H., Grauman, K., Cesa-Bianchi, N., Garnett, R. (eds.) *Advances in Neural Information Processing Systems*. vol. 31. Curran Associates, Inc. (2018), https://proceedings.neurips.cc/paper_files/paper/2018/file/69386f6bb1dfed68692a24c8686939b9-Paper.pdf
3. De Brouwer, E., Simm, J., Arany, A., Moreau, Y.: Gru-ode-bayes: Continuous modeling of sporadically-observed time series. *Advances in neural information processing systems* **32** (2019)
4. Goodwin, B.C.: Oscillatory behavior in enzymatic control processes. *Advances in enzyme regulation* **3**, 425–437 (1965)
5. Johnson, A., Pollard, T.J., Shen, L., Lehman, L.w.H., Feng, M., Ghassemi, M., Moody, B., Szolovits, P., Celi, L.A., Mark, R.G.: Mimic-iii, a freely accessible critical care database sci. *Data* **3**(160035), 10–1038 (2016)
6. Johnson, A., Bulgarelli, L., Pollard, T., Celi, L.A., Mark, R., Horng IV, S.: Mimic-iv-ed. *PhysioNet* (2021)
7. Kingma, D.P., Ba, J.: Adam: A method for stochastic optimization. *arXiv preprint arXiv:1412.6980* (2014)
8. Lloyd, C.M., Lawson, J.R., Hunter, P.J., Nielsen, P.F.: The cellml model repository. *Bioinformatics* **24**(18), 2122–2123 (2008)
9. Menne, M.J., Williams Jr, C., Vose, R.S.: United states historical climatology network daily temperature, precipitation, and snow data. *Carbon Dioxide Information Analysis Center, Oak Ridge National Laboratory, Oak Ridge, Tennessee* (2015)
10. Nie, Y., Nguyen, N.H., Sinthong, P., Kalagnanam, J.: A time series is worth 64 words: Long-term forecasting with transformers. *arXiv preprint arXiv:2211.14730* (2022)
11. Schirmer, M., Eltayeb, M., Lessmann, S., Rudolph, M.: Modeling irregular time series with continuous recurrent units. In: *International Conference on Machine Learning*. pp. 19388–19405. PMLR (2022)
12. Scholz, R., Born, S., Duong-Trung, N., Cruz-Bournazou, M.N., Schmidt-Thieme, L.: Latent linear ODEs with neural kalman filtering for irregular time series forecasting (2023), <https://openreview.net/forum?id=a-bD9-0ycs0>
13. Shukla, S.N., Marlin, B.M.: Multi-time attention networks for irregularly sampled time series. *arXiv preprint arXiv:2101.10318* (2021)
14. Silva, I., Moody, G., Scott, D.J., Celi, L.A., Mark, R.G.: Predicting in-hospital mortality of icu patients: The physionet/computing in cardiology challenge 2012. In: *2012 Computing in Cardiology*. pp. 245–248. IEEE (2012)
15. Tarasiou, M., Chavez, E., Zafeiriou, S.: Vits for sits: Vision transformers for satellite image time series. In: *Proceedings of the IEEE/CVF Conference on Computer Vision and Pattern Recognition*. pp. 10418–10428 (2023)

16. Vaswani, A., Shazeer, N., Parmar, N., Uszkoreit, J., Jones, L., Gomez, A.N., Kaiser, L., Polosukhin, I.: Attention is all you need. *Advances in neural information processing systems* **30** (2017)
17. Yalavarthi, V.K., Madusudanan, K., Sholz, R., Ahmed, N., Burchert, J., Javed, S., Born, S., Schmidt-Thieme, L.: Forecasting irregularly sampled time series using graphs (2023)